DOI 10.1007/s10946-024-10201-w
Journal of Russian Laser Research, Volume 45, Number 2, March, 2024

DESIGN AND EXPERIMENTAL STUDY OF OPTICAL SYSTEM FOR ULTRA-LOW SELF-HEATING RADIATION LONG-WAVE INFRARED LASER COMMUNICATION OPTICAL SYSTEM

Meixuan Li,[1,3] Minghui Gao,[5] Meijiao Wang,[2,4] and Feng Yang[1,3*]

[1] *Institute for Interdisciplinary Quantum Information Technology, Jilin Engineering Normal University Changchun 130052, China*

[2] *School of Optoelectronic Engineering, Changchun College of Electronic Technology Changchun 130022,China*

[3] *Jilin Engineering Laboratory for Quantum Information Technology Changchun 130052, China*

[4] *School of Materials Science and Engineering, Changchun University of Science and Technology Changchun 130022, China*

[5] *Changchun Institute of Optics, Fine Mechanics and Physics, Chinese Academy of Sciences Changchun 130033, China*

*Corresponding author e-mail: 2019200119@mails.cust.edu.cn

Abstract

In this study, we design an ultra-low self-heating radiation long-wave infrared laser communication optical system, which mainly includes aperture stop, primary mirror, secondary mirror, three-mirror, field stop, four-mirror, window glass, detector light shield, and image plane. The system enters a pupil diameter of 280 mm, a field of view angle of $1\times1^\circ$, a system focal length of 840 mm, and a wavelength of $8-12$ μmkm; the off-axis four-fold anti-structure is adopted. The optical mirror and structural components of the material are Aluminum, the system's own thermal radiation equivalent to a black-body temperature of 171 K. The equivalent black-body temperature of the system is measured in a vacuum chamber. The temperature of the spacer is 100 – 120 K, the temperature of the cold plate is 85 – 87 K, and the integration time is 550 – 800 μs. At this time, the measured equivalent black-body radiation temperature of the system is 172.9 K; it is consistent with the simulation value. The design scheme solves the technical problems of low signal-to-noise ratio, poor image contrast, and short detection distance of infrared laser communication system.

Keywords: infrared laser communication, self-radiation, optical system, signal-to-noise ratio, image contrast.

1. Introduction

As an important component of the space-based detection system, the infrared laser communication detection system has two advantages over the visible light detection system. First, the infrared optical system has passive concealment by acquiring the radiation characteristics of infrared targets and detecting the geometric or material information of targets, while visible light targets use the reflection of natural light on their own surfaces to obtain the reflected light information of targets, which is easy to be

Manuscript submitted by the authors in English on February 6, 2024.

found by monitored targets and has poor concealment [1–4]. Second, when the target of visible light surveillance is in the back shadow area of the sun, visible light detection cannot continue to monitor, while infrared detection can continue to track and monitor to avoid target loss, which can realize all-weather surveillance [5–9]. With the development of space exploration technology, infrared imaging systems have been widely used in the fields of air and space attack and defense, astronomical observation, and remote sensing to the Earth [10, 11]. The outer space environment is very different from the inner space environment, mainly due to the extremely low background temperature of the space environment and the extremely weak radiation energy of the target and background [12–14]. Thus, in the context of deep space exploration, where the space background radiation is minimal, the optical system itself becomes the main background radiation for the detector [15–18].

With the development of detector technology, such as the improvement of integration time and the reduction of self-dark current, the main factor limiting the high sensitivity of infrared detection system is the background thermal radiation of the system itself. Especially in the long-wave band, the outward radiation of optical-mechanical system (optical elements, lens barrels, support ribs, etc.) reaches the detection surface and the stray radiation is often several orders of magnitude larger than the radiation of weak signal targets. The high level of thermal radiation leads to a reduction in the signal-to-noise ratio of the detected target and a deterioration in the contrast of the image, which reduces the level of the entire image, shortens the dynamic range of the image, and the overall gray scale distribution is uneven; in serious cases, the detected target signal is flooded, and it is impossible to identify the target signal, or a false signal is detected, and the detected target may be lost, which reduces the detection efficiency, and even leads to the failure of the entire detection system [19–23].

If the thermal radiation of the optical system of the detection instrument or the components of the instrument itself in the field of view is strong, the background noises seriously affect the detection of the target by the detection instrument. Therefore, in order to improve the detection sensitivity of the infrared detection system, it is necessary to reduce the radiation intensity of the optical system of the detection instrument and the components of the instrument in the field of view, and the use of infrared ultra-low self-heating radiation optical system is currently the most important method [24–30]. It is of great application value and practical significance to study how to suppress and reduce the level of thermal radiation of the infrared optical system itself, to improve the signal-to-noise ratio of the system, and to realize long-distance infrared laser communication.

2. Optical System Design

In Fig. 1, we show the ultra-low self-heating radiation long-wave infrared optical system designed in this study, which mainly consists of the aperture diaphragm, primary mirror, secondary mirror, field-of-view diaphragm, three-mirror, four-mirror, window glass, detector mask, and image plane. Among them, the aperture diaphragm caliber is 280 mm, from the primary mirror through a light caliber center distance of 820 mm. The primary mirror for the order of 8 times is aspheric, with an aperture of 330 mm, through the back of the frame structure and the secondary mirror connected to the relative position of the fixed between them. The field of view diaphragm is located between the secondary mirror and three-mirror. The secondary mirror, three-mirror, and four-mirror are non-spherical surfaces with orders of 10, 8, and 10, respectively, with apertures of 50, 70, and 320 mm. The three-mirror is an aspheric of order 8, with an aperture of 70 mm, and made of Aluminum. The quadruple mirror is an aspheric of order 10, with an aperture of 320 mm, and made of Aluminum. The thickness of the window is 2.5 mm, the material is

Germanium, and the diameter is equal to 40 mm.

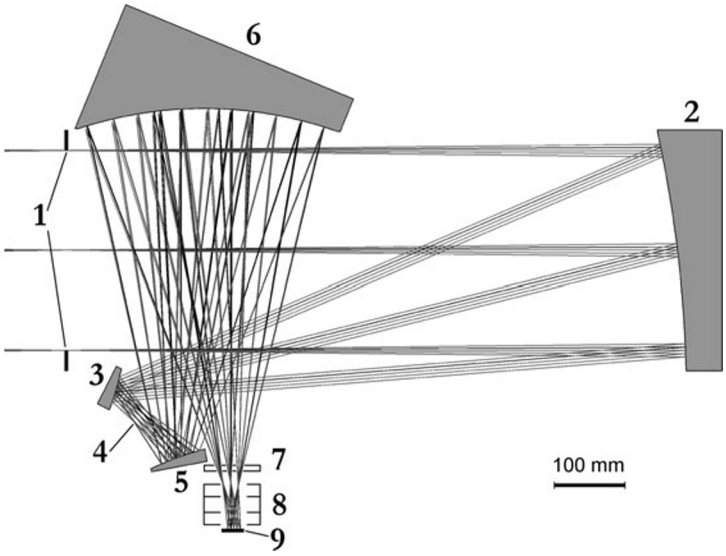

Fig. 1. Schematic diagram of the structure of the ultra-low equivalent temperature long-wave infrared laser communication optical system; here, aperture stop (1), primary mirror (2), secondary mirror (3), field stop (4), three-mirror (6), four-mirror (6), window (7), primary mirror shading hood (8), and image plane (9).

The system has an entry pupil diameter of 280 mm, a field of view of $1 \times 1^\circ$, a focal length of 840 mm, the off-axis four-reflector structure, the aberration is smaller than 1%, and the root mean square diameter of the whole field dot diagram is smaller than 25 μ. The primary, secondary, and three and four mirror surfaces are coated with Gold and dielectric reflective, and the average reflectivity of the mirrors at the wavelength of the 8.0 – 12 μ band is larger than 99.6%.

A field stop is placed at the middle image plane between the secondary mirror and the three-mirror, and Q17 matting paint developed by School of Materials, Harbin Institute of Technology is sprayed on the front surface of the field stop. The absorption rate of this paint is better than 98%, and it has been successfully applied in many aerospace models. The rear surface is coated with a gold film with a reflectivity of >98.5%. A detector light shield is placed between the detector window and the image surface, and matting paint is sprayed on the inner surface of the hood. The primary mirror, secondary mirror, field of view diaphragm, three-mirrors, four-mirrors, and structural components of the material

Table 1. Design Parameters of the Ultra-Low Self-Emission Long-Wave Infrared Optical System.

	Surface	Radius	Spacing	Surface Attribute	YSC	ZSC	ASC
Aperture Stop	1	∞	875.652		0	0	0
Primary Mirror	2	−2798.126	−825.652	Reflective	−205.971	875.653	0.000
Secondary Mirror	3	−370.959	100.000	Reflective	−246.764	50.000	−26.711
Field Stop	4	∞	99.118	Transmissive	−205.971	150.000	0.000
Three-Mirror	5	555.733	−301.590	Reflective	-266.171	249.118	−79.524
Four-Mirror	6	566.921	839.460	Reflective	156.118	410.366	−112.396
Window Front Surface	7	∞	2.500	Transmissive	−327.225	35.871	−91.440
Window Back Surface	8	∞	60.000	Transmissive	−325.729	23.456	−91.440
Image Plane	9	∞			−391.063	234.881	−91.440

are Aluminum. The specific parameters of the system with root mean square diameter smaller than 25 μ in the point sequence diagram are shown in Table 1. Among them, YSC, ZSC, and ASC represent the angle of rotation of the optical element with respect to the y, z, and x axes, respectively.

3. Imaging Quality

As shown in Fig. 2, the image quality of the long-wave infrared optical system designed in this study can be evaluated by the following two evaluation methods:

1. *Evaluation of Root Mean Square Diameter of Point Diagram*
   As shown in Fig. 2 a, the pupil plane is divided into many small panels, using the optical path calculation program, and the intersection points between the light rays passing through these panels and the image plane are calculated, which form a point array diagram. The dot sequence diagram of the ideal optical system is one point, while the dot sequence diagram of the actual optical system is countless points, and the imaging quality of the optical system is determined by the distribution of these points. The advantage is that it can understand the spatial direction of light and roughly estimate the shape of light spot. This method is commonly used to evaluate target detection in infrared systems. For the designed ultra-low self-radiation long-wave infrared optical system, we show in Fig. 2 a the point sequence diagram of each field of view, where the root mean square

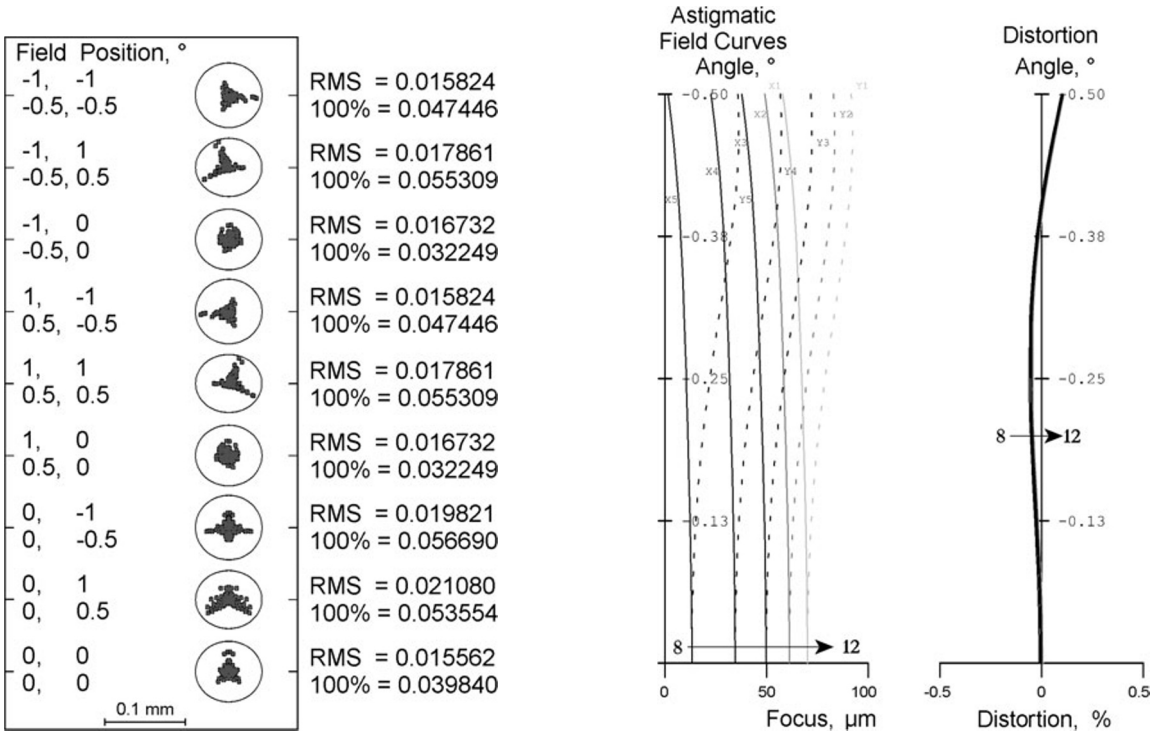

Fig. 2. The image quality of the ultra-low self-radiation long-wave infrared optical system; here, the root-mean-square diameter of point column diagram in the mid-wave infrared optical system (a) and distortion map of the long-wave infrared optical system (b). Also, curves for wavelengths of 8, 9, 10, 11, and 12 μm are shown by the arrows. Astigmatism in x direction is shown by the solid curves and y, by the dashed ones.

diameter of the dot sequence diagram is < 25 μm, which is smaller than the Airy spot diameter of the system. The imaging quality can ensure the energy concentration requirement of the long-wave infrared system, thus ensuring the requirements of long-distance laser communication.

2. *Aberration Evaluation*
   Aberration is the phenomenon known as aberration when the actual angular magnification of the main ray of light is $\neq +1$, that is, when the main ray of the image side is not parallel to the main ray of the object side, and when the point of intersection point between the main light on the image side and the ideal image plane does not coincide with the ideal image point. This phenomenon is called distortion.

In the case of distortion only, these points fall in a plane perpendicular to the optical axis, but the distance from the optical axis is incorrect. When aberrations are present, the image is clear, but misaligned. For the designed ultra-low self-radiation long-wave infrared optical system, the distortion value is shown in Fig. 2 b, and the maximum distortion value is 0.2% with the change of field of view, which meets the requirements of long-distance laser communication.

4. Optimum Design and Simulation Analysis of Self-Radiation Suppression

In the calculation of self-heating radiation of infrared optical-mechanical system, all constructed surfaces can be regarded as gray bodies or selective radiators, and the radiative outgoing degree of the build surfaces is satisfied in a finite number of wavelength bands,

$$M_\varepsilon = \varepsilon \int_{\lambda_1}^{\lambda_2} \frac{c_1}{\lambda^5} \cdot \frac{1}{\exp\left[c_2/(\lambda T)\right] - 1}\, d\lambda, \tag{1}$$

where ε is the surface emissivity of the component, $c_1 = 2\pi hc^2 = 3.7418 \cdot 10^{-16}$ W·m^2 is the first radiation constant, $c_2 = hc/k = 1.4388 \cdot 10^{-12}$ m·K is the second radiation constant, k is the Boltzmann constant, and c is the speed of light.

When the self-heating radiation on the surface of any component is transmitted in an infrared optical-mechanical system, it reaches the detector through the reflection, transmission, scattering, absorption, and diffraction at various surfaces. If the optical-mechanical system is not properly designed and the spurious radiation is not adequately suppressed, the target signal is annihilated in the stray radiation noise. In order to reduce and effectively suppress the thermal radiation level of the system itself, the following measures are mainly taken.

1. *Selection and Optimization of Optical Structure*
   Most of the researches on stray radiation and its suppression of infrared optomechanical systems focus on the pure transmission structure, two-reflection structure, and hybrid structure of refraction and reflection. Some scholars have also carried out research on off-axis three-reflection system. The research shows that under the same optical design parameters, the thermal radiation level of reflective structure is better than that of transmission structure and hybrid structure of refraction and reflection, and the off-axis reflective structure is better than that of coaxial reflective structure.

Considering the spatial layout and the position of the exit pupil, in this study, we select the off-axis four-fold optical structure. In order to reduce the influence of self-heating emission from the primary mirror, under the premise of ensuring the imaging quality, the transmission of self-heating emission from the primary mirror to the secondary mirror is reduced by controlling and reducing the aperture of the secondary mirror. The spacing between the primary and secondary mirrors is increased to reduce the spatial solid angle of the primary mirror relative to the secondary mirror, which achieves the purpose of reducing the self-heating emission of the primary mirror.

2. *Setting the Field of View Diaphragm and Detector Light Shield*
In order to effectively reduce the influence of stray light (sun, moon, etc.) outside the field of view, the surface of the system structure is treated by black dyeing process, and the emissivity of the black dyed surface is 0.86. The large-area black dyed surface greatly increases the thermal radiation of the system itself. As shown in Fig. 1, the field of view diaphragm surface is so designed that the field of view diaphragm surface is placed on the field of view diaphragm surface, and Q17 matting paint developed by the School of Materials, Harbin Institute of Technology is sprayed on the secondary mirror end to increase the absorption of stray light outside the field of view. The pupil exit surface is optimized and controlled to the back surface of the window to match the detector light shield and further suppress the influence of stray light outside the field of view.

3. *Technological Treatment of Optical Mirror Surface*
In order to reduce the radiation influence of the optical mirror, it is necessary to improve the reflectivity of the optical mirror. The technical route adopted is to coat the mirror surface with gold film and dielectric reflective. While improving the reflectivity, the optical surface can withstand the influence of cosmic rays in complex space environment, mainly the cumulative influence of space atomic Oxygen and ultraviolet radiation dose, and finally the reflectivity of the film system is optimized to 99.6%.

4. *Simulation Calculation of Radiation Equivalent Black-Body Temperature of System. Definition of Equivalent Black-Body Radiation Temperature of Optical System*
The corresponding black-body radiation temperature, when the irradiance produced by ideal black-body passing through the optical system on the image plane is equal to the irradiance produced by infrared optical system on the image plane, without considering the thermal radiation of the system. Assuming that a black-body with temperature T is placed at the entrance pupil of the optical system, the radiation flux produced by the black-body passing through the optical system on the image plane is $F_{bb}(T)$. If the influence of aberration is ignored, $F_{bb}(T)$ can be calculated by the following equation:
$$\mathrm{F_{bb}(T)} = \frac{\tau\,\pi\,L\,\mathrm{A_d}}{4\,F^2}, \tag{2}$$
where τ is the transmittance of optical system, L is the radiance of the black body, F is the number F of optical system, and the area of detector is $\mathrm{A_d}$.

According to the above equation, the corresponding relationship between the equivalent radiation temperature and radiation flux of the system is shown in Fig. 3.

Based on the 3D simulation model of thermal radiation, we calculate the order of heat radiation stray light of each component in the system image plane. The heat radiation flux of different components on

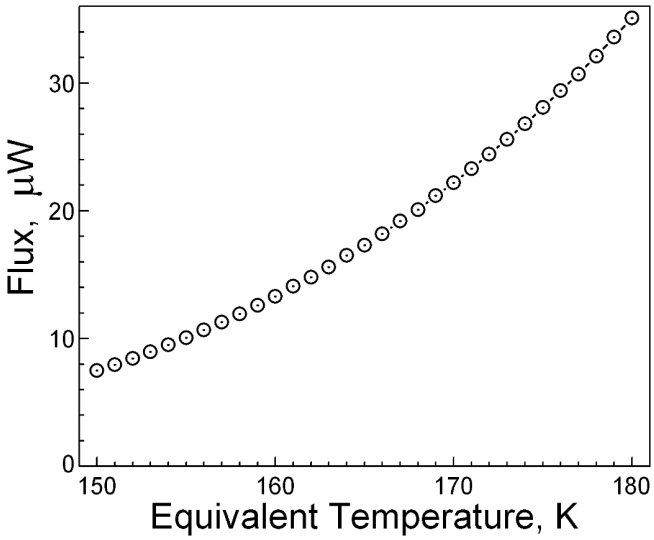

Fig. 3. Corresponding relationship between the equivalent radiation temperature and radiated flux of the system.

Table 2. Statistical Table of Thermal Radiated Flux of Each Component on the Image Plane, W.

Component Name	Thermal Radiation Flux
Primary mirror	$1.29 \cdot 10^{-7}$
Secondary mirror	$1.26 \cdot 10^{-7}$
Three-mirror	$2.71 \cdot 10^{-7}$
Four-mirror	$1.31 \cdot 10^{-6}$
Aperture stop	$8.21 \cdot 10^{-7}$
Entrance pupil	$2.01 \cdot 10^{-6}$
Exit pupil	$2.26 \cdot 10^{-7}$
Window	$8.03 \cdot 10^{-6}$
Other structural components	$1.28 \cdot 10^{-6}$
Total	$1.42 \cdot 10^{-5}$

the image plane is shown in Table 2, and the equivalent black-body temperature of the system radiation is 171 K.

5. System Equivalent Black-Body Temperature Test

Through the accurate test of the equivalent black-body temperature of the system shown in Figs. 4 and 5, the background radiation formed on the image plane can be captured, which is beneficial to the accurate calculation of the signal-to-noise ratio and detection distance of the system. The test instrumentation consists of a vacuum chamber, a background simulation board (low temperature black-body), high precision guide and adjustment table, shielding cover, optical system to be tested, detector corresponding to optical system, image acquisition software and computer, temperature sensor, and display. The vacuum chamber is shown in Fig. 4.

The test process mainly includes the following two parts.

1. *Noise Test of Detector without Optical System*
   In the linear response stage of the detector, the gray output has a linear relationship with the radiance in a certain integration time, and in the same radiance, the gray output has a linear relationship with the integration time in part of the integration time, while the gray value caused by part of the detector noise has a linear relationship with the integration time, assuming that the gray value caused by the remaining part of the noise is fixed. Therefore, only the gray DN1 output equation of the detector reads

$$\mathrm{DN1} = k\,L\,t + \mathrm{DN}_{\mathrm{noise}}\,t + \mathrm{DN0}. \tag{3}$$

   Here, k is the linear correlation index of the detector, L is the target radiation brightness, t is the integration time, $\mathrm{DN}_{\mathrm{noise}}$ is the gray value caused by the noise linearly related to the integration

Fig. 4. Test of equivalent black-body temperature of the system. Vacuum chamber equipment.

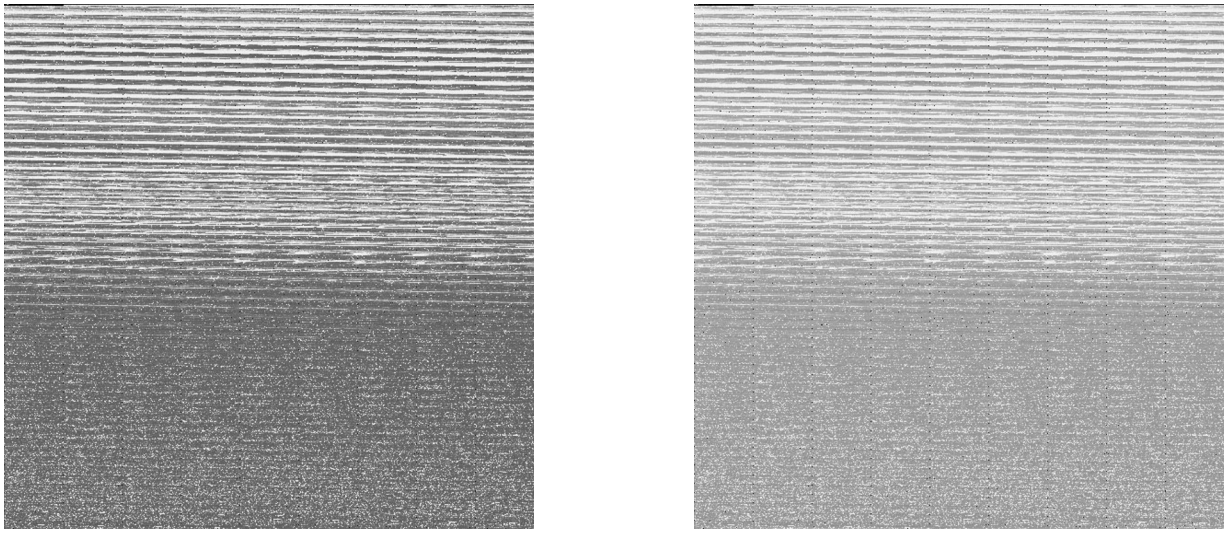

Fig. 5. Test of equivalent black-body temperature of the system; here, the gray image of detector noise background (a) and the gray image of the system (b).

time of the detector itself, and DN0 is the gray bias caused by the fixed noise of the detector. In order to cover the radiation surface of the background simulation plate in the whole field of view of the infrared camera, the infrared detector is placed in a vacuum chamber in front of the background plate with a diameter of 500 mm (small non-point source black-body can be used for single detector measurement) (no contact, interval < 5 mm). Set the temperature of the background analog plate to 125 K, 135 K, ..., 285 K, 295 K for radiometric calibration. Then K, $\mathrm{DN}_{\mathrm{noise}}$, and DN0 are solved, and the detector noise calibration is completed gray image of detector noise background; see Fig. 5a, which points out that the detector is directly facing the background simulation board under the condition of not installing the optical system, and the background simulation board generates the gray-scale image of the photoelectric signal on the surface of the detector under a certain temperature condition.

2. *Equivalent Black-Body Radiation Test with Optical System*
   The front end of the optical system is just placed in the shielding cover, and the center of the low-temperature black-body is coaxial with the optical axis of the optical system. After installing the optical system, it is assumed that the gray output of the thermal radiation of the optical system itself is a function of the integration time $\mathrm{DN}_{\mathrm{thermal}}(t)$, so the gray output equation of DN2 containing the optical system reads

$$\mathrm{DN2} = k' L\, t + \mathrm{DN}_{\mathrm{thermal}}(t) + \mathrm{DN}_{\mathrm{noise}}\, t + \mathrm{DN0}, \tag{4}$$

   where k' is the linear correlation coefficient of the optical system, and other parameters are the same as above. Calculate k' according to different temperature points, record the detector gray DN2 at this time, and calculate the corresponding temperature T_1, when the bare detector gray is DN2 by the calculation results of radiance at different temperatures in the wavelength range of 8 – 12 μ, which is the equivalent radiation temperature of the system gray image of system; see Fig. 5 b, where we show the detector and optical system integration and adjustment. In front of the optical system, in the field of view placed on the background simulation board, there are the background simulation board, the optical system at a certain temperature conditions, and the detector collected gray-scale image. Comparison can be seen in Fig. 5 a where the acquisition of the detector's background noise signal image is shown, while in Fig. 5 b the acquisition of the optical system and the detector of the two gray-scale images are shown; the difference between the two gray images is the equivalent black-body gray image of the optical system.

In test, the bulkhead temperature is 100 K – 120 K, the cold plate temperature is 85 K – 87 K, and the integration time is 550 – 800 μs. The measured equivalent black-body radiation temperature of the system is 172.9 K, which is consistent with the simulation value.

6. Conclusions

We proposed a design plan of long-wave infrared laser communication optical system with ultra-low self-radiation. By optimizing the curvature radius, aspheric coefficient, and thickness parameters of each reflector, a long-wave infrared laser communication optical system with excellent image quality and practical structural parameters was obtained. The thermal radiation of the optical system was measured under the background of low temperature, and the measured thermal radiation of the whole system was 172.9 K. Combined with the simulation results, it shows that the design plan is reliable. Self-radiation suppression measures solved the technical problems of low signal-to-noise ratio, poor image contrast, and short detection distance of infrared laser communication optical detection system.

Acknowledgments

This work was supported in part by the Science and Technology Research Project of Education Department of Jilin Province "Research on Key Technologies of Snapshot GISC Hyperspectral Satellite Remote Sensing Data Analysis and Processing" under Grant No. JJKH20240235KJ.

References

1. L. Wenhao, L. Zhaohui, M. You, et al., *Appl. Opt.*, **56**, 2428 (2017); DOI: 10.1364/ao.56.002428
2. H. Kaushal and G. Kaddoum, *IEEE Access*, **5**, 20736 (2017); DOI: 10.1109/access.2017.2755678
3. S. Hao, L. Gen, D. Yan, et al., *Laser Infrared*, **53**, 772 (2023); DOI: 10.3969/J.issn.100115078.2023.05.020
4. Schifano L, Berghmans F, Dewitte S, et al., *Sensors*, **22**, 5841 (2023); DOI: 10.3390/s22155841
5. G. Ruihong, Y. Wang, Z. Cui, et al., *Opt. Lasers Eng.*, **160**, 107287 (2023); DOI: 10.1016/j.optlaseng.2022.107287
6. L. Meixuan, K. Xiaoting, and W. Meijiao, *Laser Infrared*, **48**, 1300 (2018); DOI: 10.3969/j.issn.1001-5078.2019.01.018
7. C. Xiang-Peng, *Front. Phys.*, **9**, 731405 (2021); DOI: 10.3389/fphy.2021.731405
8. K. Renke, W. Chunping, F. Qiang, et al., *Appl. Opt.*, **62**, 398 (2023); DOI: 10.1364/ao.469807
9. B. Sahar, M. Rashid, K. Iyad, et al., *Electronics*, **11**, 1076 (2022); DOI: 10.3390/electronics11071076
10. L. Yuan, C. Wei, Z. Wang, et al., *Adv. Opt. Mater.*, **10**, 2101098 (2022); DOI: 10.1002/adom.202101098
11. C. Hui, Z. Bai, Y. Cai, et al., *Appl. Phys. Lett.*, **122**, 092202 (2023); DOI: 10.1063/5.0137542
12. N. M. Wakida, R. D. Ha, E. K. Kim, et al., *Front. Phys.*, **9**, 598930 (2001); DOI: 10.3389/fphy.2021.598930
13. C. Bin, B. Zhenxu, H. Xuanning, et al., *Opt. Express*, **31**, 5699 (2023); DOI: 10.1364/oe.480391
14. S. Fuzhou, D. Hancheng, Y. Lejun, et al., *Spectrochim. Acta A Mol. Biomol. Spectrosc.*, **280**, 121504 (2022); DOI: 10.1016/j.saa.2022.121504
15. P. Martyniuk and R. Antoni, *Light Sci. Appl.*, **11**, 6 (2022); DOI: 10.1038/s41377-022-00721-y
16. J. Duo, B. Zhenxu, L. Muye, et al., *Opt. Express*, **2**, 2942 (2023); DOI: 10.1364/oe.476759
17. G. ElMasry, R. ElGamal, N. Mandour, et al., *Food Res. Int.*, **131**, 109025 (2020); DOI: 10.1016/j.foodres.2020.109025
18. Z. Changyi, J. Yingzhuo, L. Jianzhong, et al., *Adv. Space Res.*, **69**, 823 (2022); DOI: 10.1016/j.asr.2021.09.001
19. L. Liyuan, J. Linyi, Z. Jingwen, et al., *Remote Sens.*, **14**, 1534 (2022); DOI: 10.3390/rs14071534
20. R. L. Lucke, *Opt. Eng.*, **45**, 056403 (2006); DOI: 10.1117/1.2205850
21. B. Lashkari and A. Mandelis, *Opt. Lett.*, **35**, 1623 (2010); DOI: 10.1364/ol.35.001623
22. D. M. Chandler and S. S. Hemami, *IEEE Trans. Image Process.*, **16**, 2284 (2007); DOI: 10.1109/tip.2007.901820
23. L. Jing, L. Chenguang, Z. Chongliang, et al., *Opt. Commun.*, **528**, 129052 (2023); DOI: 10.1016/j.optcom.2022.129052
24. Hermann, W.G. Friedrich, H. Andreas, et al., *J. Phys. Chem.*, **86**, 51515154 (1982); DOI: 10.1021/j100223a019
25. D. B. Sanders, *Adv. Space Res.*, **34**, 535 (2004); DOI: 10.1016/j.asr.2003.04.037
26. H. R. Wang, D. Cen, G. F. Men, and J. Y. Wang, "An infrared absorption gas detection system applying plane blazed grating," in Advanced Materials Research, Vol. 233-235, Trans Tech Publications, Ltd. (2011), pp. 2665-2668; DOI: 10.4028/www.scientific.net/amr.233-235.2665
27. M. Hirabayashi, K. Narasaki, S. Tsunematsu, et al., *Cryogenics*, **48**, 189 (2008); DOI: 10.1016/j.cryogenics.2008.03.003
28. M. J. Rieke and S. D. Horner, *Proc. SPIE*, **5904**, 590401 (2005); DOI: 10.1117/12.615554
29. Z. Xuan, Z. Gaofei, P. Ming, *Proc. SPIE*, **8193**, 819332 (2011); DOI: 10.1117/12.900688
30. L. ChenHong, *Infrared Phys. Technol.*, **107**, 103313 (2020); DOI: 10.1016/j.infrared.2020.103313